



Main Article

How soil erosion model conceptualization affects soil loss projections under climate change

Progress in Physical Geography

1–21

© The Author(s) 2019

Article reuse guidelines:

sagepub.com/journals-permissions

DOI: 10.1177/0309133319871937

journals.sagepub.com/home/ppg



Joris P.C. Eekhout 

CEBAS-CSIC, Spain

Joris De Vente

CEBAS-CSIC, Spain

Abstract

Climate models project increased extreme precipitation for the coming decades, which may lead to higher soil erosion in many locations worldwide. Different soil erosion model concepts are used to assess the impact of climate change on soil erosion at large spatial scales, including models forced by precipitation and by runoff. However, there is little knowledge of the implications of soil erosion model conceptualization on projected soil erosion rates under climate change. Here, we assess the impact of climate change with the three most widely used soil erosion model concepts: a model forced by precipitation (RUSLE); a model forced by runoff (MUSLE); and a model forced by precipitation and runoff (MMF). We applied the models to two contrasting Mediterranean catchments (south-east Spain), where climate change is projected to decrease the annual precipitation sum and increase extreme precipitation, based on the RCP8.5 climate change scenario. Depending on the model, soil erosion is projected to decrease (RUSLE) or increase (MUSLE and MMF) in the study area. Although it is difficult to validate future model projections, the differences between the model projections are, inherently, a result of their model conceptualization: a decrease in soil loss due to a decrease in the annual precipitation sum (RUSLE); and an increase in soil loss due to an increase in extreme precipitation and, consequently, increased runoff (MUSLE). An intermediate result is obtained with MMF, in which a projected decrease in detachment by raindrop impact is counteracted by a projected increase in detachment by runoff. We conclude that in climate change impact assessments it is important to select a soil erosion model that is forced by both precipitation and runoff, which under climate change may have a contrasting effect on soil erosion.

Keywords

Climate change, impact assessments, soil erosion, modelling, precipitation intensity, runoff

I Introduction

Climate change is projected to cause an increase in extreme precipitation in many locations worldwide (Sun et al., 2007), which may lead to higher soil erosion globally (Nearing et al.,

Corresponding author:

Joris P.C. Eekhout, CEBAS-CSIC, Campus Universitario Espinardo, PO Box 164, Murcia 30100, Spain.
Email: joriseekhout@gmail.com

2004). To study the impact of climate change on soil erosion, a number of different soil erosion models are applied. These erosion models use different model concepts, which is foremost expressed by the forcing used and determines which soil erosion processes are accounted for, such as raindrop splash, sheet, rill and (ephemeral) gully erosion. The two principal soil erosion processes that are responsible for most hillslope erosion are detachment by raindrop impact and detachment by runoff (Morgan, 2005). Despite numerous plot and rainfall simulation studies (e.g. Mahmoodabadi and Sajjadi, 2016; Martínez-Murillo et al., 2013; Ziadat and Taimeh, 2013), there is still limited knowledge about how hillslope erosion is affected by climate change and what the implications are for soil erosion model projections that are forced by either precipitation or runoff, or a combination of the two.

Detachment by raindrop impact is a function of the amount and size of the raindrops that reach the soil surface (Morgan, 2005). High-intensity precipitation consisting of large drops often causes most soil erosion (Nearing et al., 1990). This notion was applied in many empirical soil erosion models, which are in most cases forced by precipitation to determine soil loss. Examples of such empirical models are the Universal Soil Loss Equation (USLE) (Wischmeier and Smith, 1978), the Revised Universal Soil Loss Equation (RUSLE) (Renard et al., 1997) and the Erosion Potential Method (EPM) (Gavrilović, 1972). RUSLE is the most applied empirical model for assessing the impact of climate change at large spatial scales, based on a review of climate change impact studies (Table S1). RUSLE consists of a simple equation with a range of multiplicative factors, of which the rainfall erosivity factor (R factor) is mostly affected by climate change. The crop and management factor and the erosion control practice factor may also be affected by changes in vegetation cover, land use and management, but few studies have considered this yet. Even though

the original RUSLE utilizes the 30-minute rainfall intensity to determine rainfall erosivity, most climate change assessments apply regression models forced with monthly or annual precipitation sum to obtain the future projected rainfall erosivity (Table S1). This temporal aggregation is mainly due to a lack of future estimates of the 30-minute rainfall intensity, because most climate model output is available at a daily time step at best. As a result, most RUSLE studies project a change of soil loss equivalent to the projected change in the annual precipitation sum (e.g. Amanambu et al., 2019; Correa et al., 2016; Gupta and Kumar, 2017; Maina et al., 2013; Mondal et al., 2016; Teng et al., 2018; Zare et al., 2016).

Detachment by runoff is accounted for in many process-based soil erosion models, which are often embedded in hydrological models to simulate (surface) runoff generation (Morgan, 2005). Runoff generation depends on surface and sub-surface hydrological processes and is a function of precipitation volume and intensity, soil moisture, soil hydraulic properties and vegetation cover (Kirkby, 1988). Because of this complexity, process-based models require many input data and include many model parameters. Examples of process-based models that are forced by runoff are CAESAR (Coulthard and Van De Wiel, 2007), PESERA (Kirkby et al., 2008), STREAM (Cerdan et al., 2002), SWAT (Arnold et al., 2012) and TETIS (Bussi et al., 2014). SWAT uses the Modified Universal Soil Loss Equation (MUSLE) (Williams, 1995) to calculate soil loss, and in our review of modelling studies appeared as the most applied soil erosion model in climate change assessments (Table S1). Because MUSLE only determines detachment from runoff and not from raindrop impact, total soil loss may be underestimated, for example, in tropical climates that are dominated by high-intensity rainfall events during the monsoon season and which are responsible for high soil losses (Phomcha et al., 2011; Shrestha et al., 2013).

Hence, in climate change impact studies, increasingly, process-based models are being applied that are forced by both precipitation and runoff to account for a larger number of soil erosion processes (Figure S1). Some examples of these are ANSWERS (Beasley et al., 1980), EUROSEM (Morgan et al., 1998), INCA (Lazar et al., 2010), MEDRUSH (Kirkby et al., 1998), MEFIDIS (Nunes et al., 2005), RHEM (Nearing et al., 2011), SHETTRAN (Ewen et al., 2000), SPHY-MMF (Eekhout et al., 2018b) and WEPP (Nearing et al., 1989).

In previous studies, soil loss predictions from soil erosion models have been compared with measured plot data (Bhuyan et al., 2002; Centeri et al., 2009; Chandramohan et al., 2015; Croke and Nethery, 2006; Stolpe, 2005; Tiwari et al., 2000) and sediment yield observations at the catchment outlet (Jetten et al., 2003; Shen et al., 2009). These studies showed mixed results in model performance between empirical and process-based soil erosion models. For example, some studies showed that empirical models performed better (e.g. Chandramohan et al., 2015; Tiwari et al., 2000), whereas others showed the opposite (e.g. Croke and Nethery, 2006; Stolpe, 2005). Previous model comparison studies give valuable insight into the performance of various soil erosion models, but were mainly focused on small spatial scales, often leading to context-specific conclusions for the study site (e.g. Stolpe, 2005; Tiwari et al., 2000). Furthermore, although various previous model comparison studies included at least one process-based model forced by both precipitation and runoff, none explicitly showed how the two related soil erosion processes contributed to total soil loss and what the differences are with respect to models that are only forced by either precipitation or runoff.

Many previous studies aimed to assess the impact of climate change on soil erosion using a large variety of models forced by precipitation and/or runoff. However, there is still insufficient insight with regard to the effect of model

conceptualization on the prediction of soil erosion under climate change. Therefore, in this study, we aim to assess how differences in soil erosion model conceptualization affect soil loss projections under climate change. We compare the two most widely used soil erosion models applied in large-scale climate change assessments (i.e. RUSLE and MUSLE) and a novel process-based soil erosion model (SPHY-MMF). The three models are applied to two contrasting Mediterranean catchments, where climate change is projected to cause a significant decrease in the annual precipitation sum and increased extreme precipitation, respectively.

II Material and methods

I Study area

This study was performed in two similarly sized sub-catchments of the Segura river basin (Figure 1 and Table 1) in south-east Spain. The two catchments mainly differ in climate and land use. The Sierra de Segura catchment is predominantly classified as Mediterranean (dry summer), with an average annual precipitation sum of 544 mm between 1981 and 2000 (Serrano-Notivoli et al., 2017). It can be considered a semi-natural catchment, where forest (45.0%) and shrubland (39.6%) are the most dominant land use classes. The Guadalentín catchment is predominantly classified as semi-arid, with an average annual precipitation sum of 295 mm between 1981 and 2000 (Serrano-Notivoli et al., 2017). It can be considered an agricultural catchment, with a total agricultural cover of 43.3%, divided between cereals (17.5%), tree crops (16.9%), horticulture (8.1%) and vineyards (0.9%).

2 Soil erosion models

We have applied three soil erosion models that allow for the calculation of hillslope erosion at large spatial scales, accounting for upslope

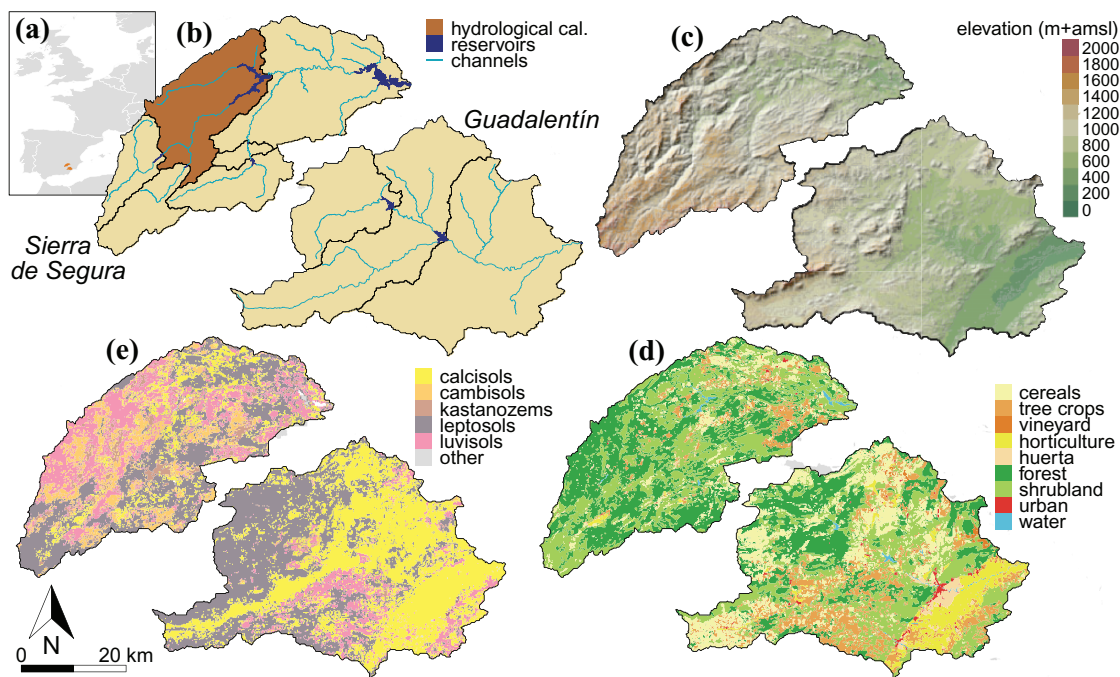


Figure 1. Location and characteristics of the Sierra de Segura and Guadalentín catchments: (a) location of the catchment within Europe; (b) the hydrological calibration area (brown); the channels (light blue), and the reservoirs (dark blue); (c) Digital Elevation Model (Farr et al. 2007); (d) land use map (MAPAMA, 2010); and (e) soil type map (Hengl et al., 2017).

Table 1. Catchment characteristics.

	Sierra de Segura	Guadalentín
area (km^2)	2589.04	2628.68
mean annual precipitation sum (mm)	544.4	294.9
average temperature (C)	13.24	14.73
average slope (m/m)	0.146	0.095
dominant Köppen class (area)	Cs (67.2%)	BS (86.9%)
cereals (%)	7	17.5
tree crops (%)	6.4	16.8
vineyard (%)	0.2	0.9
horticulture (%)	0.4	8.1
huerta (%)	0.6	1.5
forest (%)	45.0	22.7
shrubland (%)	39.6	30.7
urban (%)	0.3	1.2
water (%)	0.5	0.6

contributing area and runoff. Throughout the article we only use the cells with a contributing area smaller than 2 km^2 , because in cells with a larger contributing area other soil erosion processes may dominate, for example, gully and channel bank erosion, which are not accounted for in the three soil erosion models. Although the study applies the soil erosion models at the catchment scale, we do not evaluate their predictions of catchment-scale suspended sediment yields.

2.1 RUSLE. RUSLE is an empirical model consisting of five factors that describe the climate (rainfall erosivity), soil erodibility, topography (slope length and steepness), crop management and conservation practice. The model was originally developed for application at the hillslope scale, but is frequently applied from hillslopes

to large catchments and even globally (e.g. Borrelli et al., 2017; Liu et al., 2019; Panagos et al., 2015). The RUSLE model is described as (Renard et al., 1997)

$$E = R K L S C P \quad (1)$$

where E is the mean annual soil loss ($\text{t ha}^{-1} \text{y}^{-1}$), R is the rainfall erosivity factor ($\text{MJ mm m}^{-2} \text{h}^{-1} \text{yr}^{-1}$), K is the soil erodibility factor ($\text{kg h MJ}^{-1} \text{mm}^{-1}$), LS is the topographic factor (-), C is the crop and management factor (-) and P is the erosion control practice factor (-).

We assessed the rainfall erosivity R factor from the average monthly precipitation using the method suggested by Renard and Freimund (1994)

$$R = \begin{cases} 0.7397 MFI^{1.847}, & \text{if } MFI < 55\text{mm} \\ 95.77 - 6.081 MFI + 0.4770 MFI^2, & \text{if } MFI > 55\text{mm} \end{cases} \quad (2)$$

where MFI is the Modified Fournier Index (mm), defined by (Arnoldus, 1977)

$$MFI = \frac{\sum_{i=1}^{12} p_i^2}{P} \quad (3)$$

where p_i is the average monthly precipitation (mm) and P is the average annual precipitation (mm).

The soil erodibility factor was determined using the equation developed by Wischmeier et al. (1971)

$$K = \frac{0.00021 M^{1.14} (12 - OM) + 3.25(c_{\text{soilstr}} - 2) + 2.5(c_{\text{perm}} - 3)}{100} \quad (4)$$

where M is the particle-size parameter (-), OM is the organic matter content (%), c_{soilstr} is the soil structure class (-) and c_{perm} is the profile permeability class (-). The particle-size parameter is calculated as follows

$$M = (m_{\text{silt}} + m_{\text{vfs}})(100 - m_c) \quad (5)$$

where m_{silt} is the silt content (%), m_{vfs} is the very fine sand content (%) and m_c is the clay content (%).

The profile permeability classes are defined according to the saturated hydraulic conductivity, which was determined from pedotransfer functions (Saxton and Rawls, 2006). The silt, clay and organic matter content were obtained from the SoilGrids database (Hengl et al., 2017). Due to the absence of data, we set $m_{\text{vfs}} = 0$ and $c_{\text{soilstr}} = 2$, which corresponds to the fine granular class.

The topographic LS factor is often determined by a multiplication of the slope length L factor and slope steepness S factor. To represent the flow accumulation, we applied the method proposed by Desmet and Govers (1996) to determine the L factor

$$L = \frac{(A + D^2)^{m+1} - A^{m+1}}{D^{m+2} x^m 22.13^m} \quad (6)$$

where A is the contributing area at the inlet of the grid cell (m^2), D is the grid cell size (m^2), m is an coefficient (-) and x is defined as

$$x = \sin\alpha + \cos\alpha \quad (7)$$

where α is the aspect direction of the grid cell. The coefficient m is determined as follows

$$m = \frac{\beta}{(1 + \beta)} \quad (8)$$

$$\beta = \frac{\sin \theta / 0.0896}{3(\sin \theta)^{0.8} + 0.56} \quad (9)$$

where θ is the slope angle.

We applied the method proposed by McCool et al. (1987) to determine the S factor

$$S = \begin{cases} 10.8 \sin \theta + 0.03, & \text{if } \theta < 9\% \\ 16.8 \sin \theta - 0.5, & \text{if } \theta \geq 9\% \end{cases} \quad (10)$$

The crop and management factor that represents the reducing effect of vegetation on soil loss was used in the calibration procedure and the erosion control practice factor was set to 1.

2.2 MUSLE. MUSLE is a modification of the USLE in which the rainfall erosivity factor is replaced by a runoff factor and applied at a daily time step. MUSLE is incorporated into various widely used hydrological models, such as SWAT, in which a separate hydrological module is used to calculate runoff. MUSLE is determined as follows (Williams, 1995)

$$sed = 11.8(Q_{surf}q_{peak}A)^{0.56} K LS C P CFRG \quad (11)$$

where sed is the sediment yield ($\text{kg m}^{-2} \text{ day}^{-1}$), Q_{surf} is the surface runoff depth (mm), q_{peak} is the peak runoff rate ($\text{m}^3 \text{ s}^{-1}$), A is the cell area (m^2), K is the soil erodibility factor ($\text{kg h MJ}^{-1} \text{ mm}^{-1}$), LS is the topographic factor (-), C is the crop and management factor (-), P is the erosion control practice factor (-) and $CFRG$ is the coarse fragment factor (-). The soil erodibility factor, the crop and management factor and the erosion control practice factor were determined by the methods described under RUSLE.

The surface runoff Q_{surf} is determined with the hydrological model SPHY as described in Section 3. The peak runoff rate is determined as follows

$$q_{peak} = \frac{\alpha_{tc} Q_{surf} A}{3.6 t_{conc}} \quad (12)$$

where α_{tc} is the fraction of daily rainfall that occurs during the time of concentration (-) and t_{conc} is the time of concentration (hr). The time of concentration is defined as the amount of time from the beginning of a rainfall event until the entire cell area is contributing to flow at the cell outlet.

The fraction of daily rainfall that occurs during the time of concentration is determined as follows

$$\alpha_{tc} = 1 - \exp[2t_{conc} \ln(1 - \alpha_{0.5})] \quad (13)$$

where $\alpha_{0.5}$ is the fraction of the daily rain falling in the half-hour of highest intensity (-), which is obtained from a model parameter in the hydrological model and is determined within the

calibration of the hydrological model. The time of concentration is determined, accounting for both channel flow (Kirpich, 1940) and overland flow (Kerby, 1959).

The coarse fragment factor is determined as follows

$$CFRG = \exp(-0.053p_{rock}) \quad (14)$$

where p_{rock} is the rock content in the root zone layer (%) that was obtained by applying the empirical formulations from Poesen et al. (1998), which determine rock fraction based on slope gradient.

The topographic factor is the expected ratio of soil loss per unit area from a field slope to that from a 22.1 m length of uniform 9% slope. We applied the following equation (Wischmeier and Smith, 1978)

$$LS = \left(\frac{L_{hill}}{22.1} \right)^m (65.41 \sin^2(\alpha_{hill}) + 4.56 \sin \alpha_{hill} + 0.065) \quad (15)$$

where L_{hill} is the slope length (m), m is an exponential term (-) and α_{hill} is the slope angle ($^\circ$). The exponential term m is calculated as follows

$$m = 0.6(1 - \exp[-35.835S]) \quad (16)$$

where S is the slope (m/m).

2.3 MMF. Morgan–Morgan–Finney (MMF) is a process-based soil erosion model (Morgan and Duzant, 2008) that we fully integrated with the SPHY hydrological model. See Section 3 for a summary of the hydrological component and Eekhout et al. (2018b) for a full description of the SPHY-MMF model. To determine soil loss, MMF receives input from the SPHY model, for example, effective precipitation (throughfall), runoff and canopy cover.

Detachment of soil particles is determined separately for raindrop impact and runoff. The detachment of soil particles by raindrop impact F (kg m^{-2}) is determined as follows

$$F_i = K_i \frac{\%i}{100} (1 - GC) KE \times 10^{-3} \quad (17)$$

where K_i is the detachability of the soil by raindrop impact (g J^{-1}), i is the textural class, that is, c for clay, z for silt and s for sand, GC is the ground cover (-) and KE is the kinetic energy of the effective rainfall (J m^{-2}).

The kinetic energy of the effective rainfall is determined separately for direct throughfall and leaf drainage, and is subsequently summed to obtain the total rainfall energy. Canopy cover, which is obtained from the dynamic vegetation module within the hydrological model, is used to separate direct throughfall and leaf drop from effective precipitation. The ground cover protects the soil from detachment and includes the proportion of vegetation and rocks covering the surface; it is set to 1 in case of the presence of snow. The spatially distributed rock fraction map was obtained by applying the empirical formulations from Poesen et al. (1998), which determine rock fraction based on slope gradient.

Here, we apply an adapted version of SPHY-MMF, in which the kinetic energy of the direct throughfall (KE_{DT} , J m^{-2}) is based on a relationship described by Brown and Foster (1987), which has also been applied in other soil erosion studies in Spain (e.g. Angulo-Martínez et al., 2016; Beguería et al., 2018)

$$KE_{DT} = DT(0.29(1 - 0.72\exp(-0.05I))) \quad (18)$$

where DT is the direct throughfall (mm) and I is the intensity of the erosive precipitation (mm h^{-1}). The intensity of the erosive precipitation is obtained from the hydrological model, which uses the fraction of daily rainfall that occurs in the hour with the highest intensity to determine infiltration excess surface runoff. This fraction was used in the calibration of the hydrological model.

The detachment of soil particles by runoff H (kg m^{-2}) is determined as follows

$$H_i = DR_i \frac{\%i}{100} Q^{1.5} (1 - GC) \sin^{0.3} S \times 10^{-3} \quad (19)$$

where DR is the detachability of the soil by runoff (g mm^{-1}), Q is the volume of accumulated runoff (mm) and S is the slope angle ($^\circ$).

Subsequently, the detachment of soil particles by raindrop impact (F) and runoff (H) are summed. Only a fraction of the detached soil will be delivered to the runoff for transport; the remainder will be deposited immediately, that is, within the cell of its origin. The fraction of the detached sediment that is deposited immediately is estimated from the particle fall number (Tollner et al., 1976)

$$DEP_i = 44.1 N_f^{0.29} \quad (20)$$

where N_f is the particle fall number, which is a function of the presence and abundance of vegetation and the surface roughness.

The amount of soil particles that will be taken into transport is calculated as follows

$$G = \sum_i (F_i + H_i)(1 - (DEP_i/100)) \quad (21)$$

Whereas vegetation characteristics in RUSLE and MUSLE are based mainly on a single model parameter (C-factor), MMF requires a number of model parameters to parameterize vegetation characteristics. For instance, for each land use class the user needs to specify the plant height, stem diameter, stem density and the ground cover fraction. Furthermore, vegetation characteristics are temporally dynamic to represent intra-annual vegetation development through the canopy cover and an optional sowing–harvest cycle, here implemented for cereals and horticulture. For land use classes for which no stem diameter and stem density values are available, for example, because of an irregular distribution of the vegetation, the user can provide the Manning roughness coefficient for vegetation, here implemented for forest and shrubland.

3 Hydrological model

MUSLE and MMF are forced with accumulated runoff from a hydrological model. Here, we

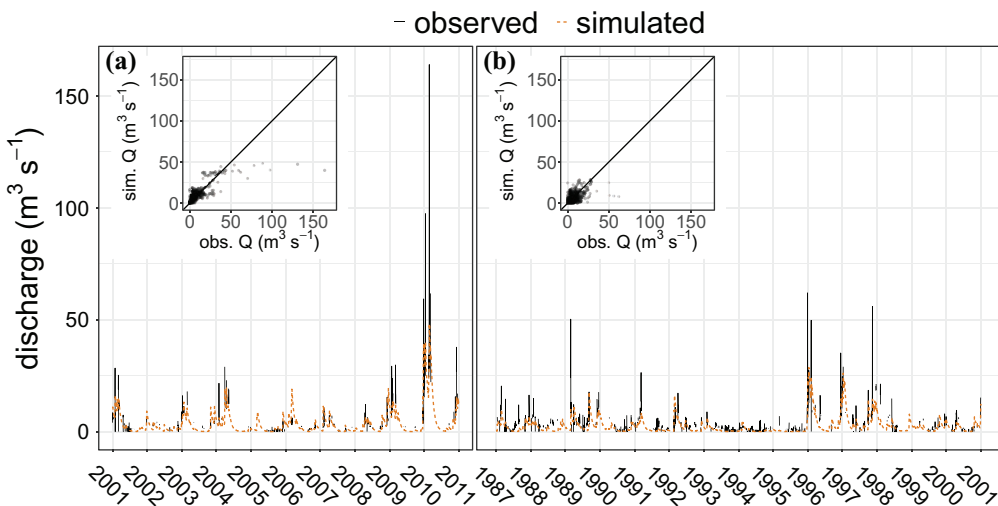


Figure 2. Discharge time series for the calibration (a) and validation period (b). The solid line corresponds to the observed time series and the dashed orange line corresponds to the simulated time series. The small insets show the offset between observed and simulated discharge.

applied the SPHY model (v3.0) (Eekhout et al., 2018b; Terink et al., 2015), a spatially distributed hydrological model. We employed a model grid with a resolution of 200 m. The hydrological model simulates most relevant hydrological processes such as interception, evapotranspiration, surface runoff, and lateral and vertical soil moisture flow. The model also incorporates a vegetation module, which determines actual evapotranspiration, interception, canopy storage, throughfall and canopy cover, based on the spatial and temporal variation of the Normalized Differenced Vegetation Index (NDVI). No NDVI images were available for the reference and the future periods, therefore, we determined NDVI based on a land use-specific log-linear relationship between NDVI and climate conditions (precipitation and temperature) obtained from a calibration period (2000–2012), as described in detail in Eekhout et al. (2018a).

The hydrological model was calibrated in the Fuensanta sub-catchment (Sierra de Segura) for the period 2001–2010 and validated for the period 1987–2000 using daily observed

discharge data. Extreme precipitation events have most impact on soil erosion (Nearing et al., 1990), hence, we focused the calibration and validation procedure on the largest discharge events. We used a baseflow separation algorithm to separate large discharge events from the rest of the time series using the method proposed by Ladson et al. (2013), with $\alpha = 0.925$. We used a threshold of twice the calculated baseflow to separate the discharge events, which occur in 19% of the time. We applied the SPOTPY calibration package (Houska et al., 2015) to calibrate the hydrological model, using the simulated annealing algorithm to optimize the Nash–Sutcliffe model efficiency (NSE) (Nash and Sutcliffe, 1970). The calibration resulted in a NSE of 0.60 and the validation in a NSE of 0.32 for daily discharge (Figure 2).

4 Climate data

We applied the three erosion models to a reference scenario (1981–2000) and two future climate scenarios from one Representative

Table 2. The nine climate models used in this study, with their corresponding RCM, GCM and research institute.

GCM	RCM				
	CCLM ^a	HIRHAM5 ^b	RACMO ^c	RCA ^d	WRF ^e
CNRM-CM5	×				×
EC-EARTH	×	×	×		×
IPSL-CM5A-MR					×
MPI-ESM-LR	×				×

^aClimate Limited-area Modelling Community (CLMcom).

^bDanish Meteorological Institute (DMI).

^cRoyal Netherlands Meteorological Institute (KNMI).

^dSwedish Meteorological and Hydrological Institute (SMHI).

^eInstitut Pierre Simon Laplace (IPSL).

GCM: general circulation model; RCM: regional climate model.

Concentration Pathway (RCP8.5), reflecting a continued rise of greenhouse gas emissions throughout the 21st century. The two scenarios are divided between two future periods, that is, 2031–2050 (near future scenario) and 2081–2100 (far future scenario). We obtained data from a total of nine climate models (GCM/RCM combinations – see Table 2) from the EURO-CORDEX initiative (Jacob et al., 2014), with a 0.11° resolution. Precipitation data for the reference period (1981–2000) were obtained from the SPREAD daily dataset (Serrano-Notivoli et al., 2017), with a 5 km resolution. Temperature data for the reference period were obtained from the Spain02 daily dataset (Herrera et al., 2016), with a 0.11° resolution. Precipitation and temperature data were interpolated on the model grid using bilinear interpolation. The climate model data were bias-corrected using scaled distribution mapping (SDM) (Switanek et al., 2017). This bias correction method scales the observed precipitation distribution by raw model projected changes in magnitude, rain day frequency and likelihood of events. Eekhout and Vente (2019) showed that SDM best reproduces the projected climate change signal in the study area.

5 Uncertainty analysis

To account for uncertainty, we evaluated the significance of the climate projections and the model predictions within the ensemble of nine climate models. A paired U-test (Mann–Whitney–Wilcoxon test, with a significance level of 0.05) was applied to test the significance of model outcomes for the nine climate models. The pairs consisted of the model output for (a) the reference scenario and (b) the nine climate models. The paired U-test was also applied to determine the significance of the catchment-averaged change with respect to the reference scenario.

III Results

I Calibration and validation

The soil erosion models were calibrated for the period 2001–2010 and validated for the period 1981–2000 using plot-scale soil loss data for the Mediterranean region (Maetens et al., 2012). We determined the annual unit soil loss (SL_u), which is soil loss corrected for plot length and slope gradient. In the calibration procedure, the model parameters were adjusted such that the average soil loss per land use class was within 1% of the literature values (see last column of Table 4). The RUSLE and MUSLE models were calibrated with land use-specific values for the C factor

Table 3. Calibration parameters of the three soil erosion models.

Land use Class	RUSLE	MUSLE	MMF					
	C factor (-)	C factor (-)	PH (m)	NV (stems m ⁻²)	D (m)	GC (-)	Manning (s m ^{-1/3})	Other ^a
cereal	0.053	0.14	0.75	400	0.0235	0.22	n/a	T
(harvested) ^b	n/a	n/a	0	0	0	0	n/a	T
huerta	0.068	0.149	0.5	500	0.01	0.45	n/a	T
horticulture	0.14	0.118	0.3	6.25	0.347	0.75	n/a	T
(harvested) ^b	n/a	n/a	0	0	0	0	n/a	T
tree crops	0.073	0.225	2	n/a	n/a	< 0.01	n/a	T, N.V.
vineyard	0.132	0.217	1	n/a	n/a	0.02	n/a	T, N.V.
forest	0.00045	0.0185	10	n/a	n/a	0.637	0.2 ^c	
shrubland	0.0042	0.0405	0.5	n/a	n/a	0.69	0.1 ^c	
urban/water	0	0	0	0	0	0	n/a	N.E.

^aT represents tillage, N.E. represents no erosion, N.V. represents no vegetation.

^bSubject to sowing–harvest cycle in MMF, with sowing on day 288 and harvest on day 166.

^cObtained from Chow (1959).

RUSLE: Revised Universal Soil Loss Equation; MUSLE: Modified Universal Soil Loss Equation; MMF: Morgan–Morgan–Finney.

Table 4. Validation of annual unit soil loss and comparison with literature data (Mg km⁻² yr⁻¹).

Land use class	RUSLE	MUSLE	MMF	Maetens et al. (2012)
cereals	185.4	205.2	161.0	230.0
huerta	224.8	214.2	232.0	230.0
horticulture	242.7	202.9	211.0	230.0
tree crops	224.4	247.5	341.0	300.0
vineyard ^a	183.9	319.5	238.0	300.0
forest ^b	29.8	31.1	31.0	40.0
shrubland	22.8	24.7	25.0	30.0
urban/water	0.0	0.0	0.0	n/a.

^aAnnual unit soil loss not available, used the value of tree crops instead.

^bAnnual unit soil loss not available, used annual soil loss instead.

RUSLE: Revised Universal Soil Loss Equation; MUSLE: Modified Universal Soil Loss Equation; MMF: Morgan–Morgan–Finney.

(Table 3). For MMF we used two land use classes as a baseline (tree crops and vineyard). These two land use classes are assumed to have negligible ground cover due to frequent ploughing, hence, the land use-specific model parameters do not affect their soil loss. With these two land use classes, we calibrated the detachability of the soil by raindrop impact (K from equation (17)) and the detachability of the soil by runoff (DR from

equation (19)). Then, we calibrated the other land use classes with ground cover, stem diameter and stem density. Table 4 shows the validation results of the three soil erosion models.

2 Climate signal

Climate change will significantly affect the climate signal in the two catchments. A significant

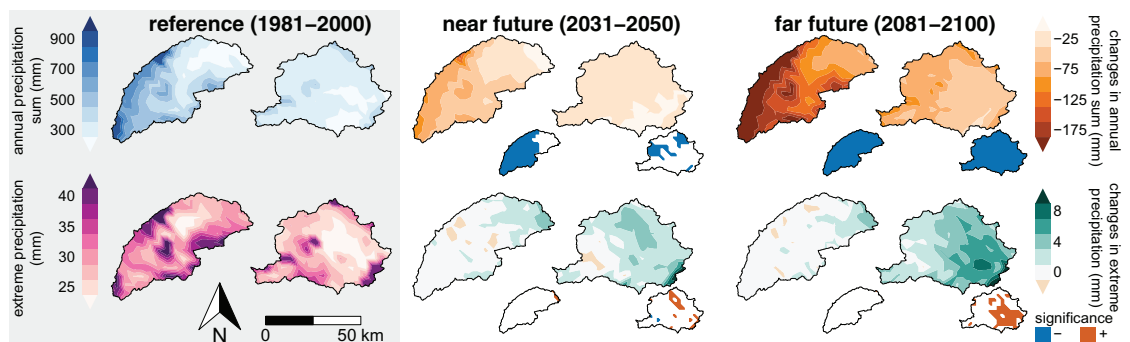


Figure 3. Ensemble average annual precipitation sum (mm, upper row) and ensemble average extreme precipitation (mm, lower row) defined as the 95th percentile of daily precipitation, considering only rainy days ($> 1 \text{ mm day}^{-1}$) (Jacob et al., 2014), for the reference scenario (left) and changes between the reference scenario and the two future scenarios (right). The small maps in the bottom right-hand corner of each map represent the significance, where blue indicates a significant decrease and red a significant increase ($p < 0.05$).

Table 5. Catchment-averaged annual precipitation sum (mm), extreme precipitation (mm) and average temperature ($^{\circ}\text{C}$) from the reference scenario and difference between the reference and the future scenarios. The catchment-averaged projections are accompanied by percentages in parentheses, except for average temperature. Values marked in bold are significantly different from zero ($p < 0.05$).

	Sierra de Segura			Guadalentín		
	reference (1981-2000)	near future (2031-2050)	far future (2081-2100)	reference (1981-2000)	near future (2031-2050)	far future (2081-2100)
prec. sum (mm)	544.4	-48.7 (-9.0)	-147.2 (-27.0)	294.9	-17.6 (-6.0)	-61.7 (-20.9)
extr. prec. (mm)	31.77	0.48 (1.5)	0.36 (1.1)	30.53	1.92 (6.3)	3.86 (12.7)
avg. temp. ($^{\circ}\text{C}$)	13.24	1.56	4.43	14.73	1.40	4.05

prec.: precipitation; extr. prec.: extreme precipitation; avg. temp.: average temperature.

decrease in the annual precipitation sum is projected in the Sierra de Segura catchment for both scenarios (Figure 3 and Table 5), up to a catchment-averaged decrease of 147 mm (-27.0%) in the far future scenario. In the Guadalentín catchment, a catchment-averaged decrease is projected, but is only significant in the far future scenario, with a decrease of 61.7 mm (-20.9%).

The change in extreme precipitation is a crucial climate signal for soil erosion impact assessments. An increase in extreme precipitation is projected in the two catchments, with a small increase in the Sierra de Segura catchment and a large increase in the Guadalentín

catchment. In the Guadalentín catchment, a significant increase in extreme precipitation is projected in parts of the catchment, most notably in the far future scenario in the south-eastern part of the catchment. Furthermore, a significant increase in average temperature is projected in the two catchments, with an increase of 1.4 – 1.6 $^{\circ}\text{C}$ in the near future scenario and 4.1 – 4.4 $^{\circ}\text{C}$ in the far future scenario.

3 Soil loss projections

For the reference scenario, each model projects a different spatial pattern in soil loss (Figure 4).

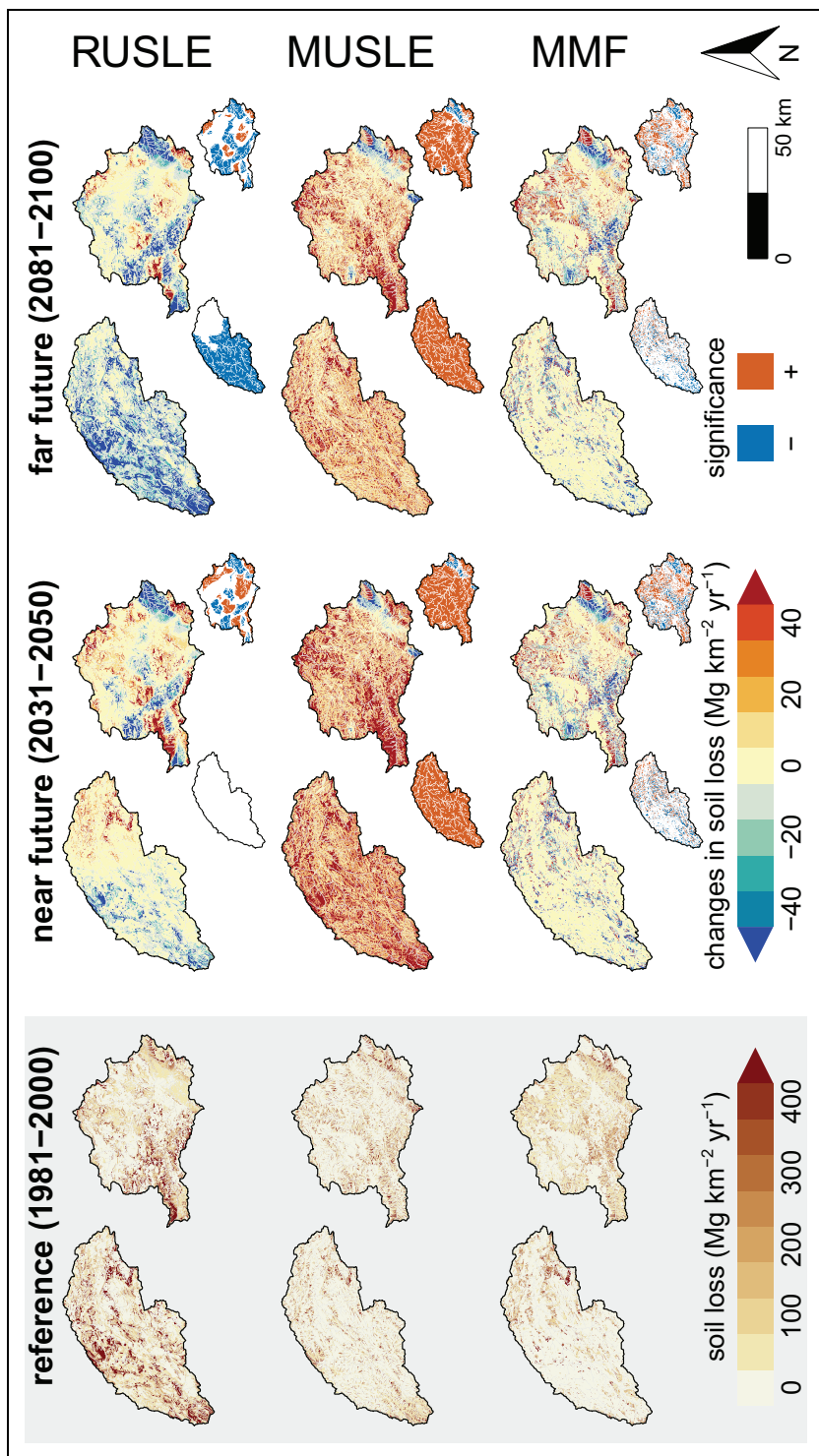


Figure 4. Ensemble average annual soil loss ($\text{Mg km}^{-2} \text{yr}^{-1}$) for each soil erosion model, for the reference scenario (1981–2000 left) and changes between the reference scenario and the two future scenarios (2031–2050 middle; 2081–2100 right). The small maps in the bottom right-hand corner of each map represent the significance, where blue indicates a significant decrease and red a significant increase ($p < 0.05$).

Table 6. Catchment-averaged annual soil loss ($\text{Mg km}^{-2} \text{yr}^{-1}$) for each soil erosion model from the reference scenario and difference between the reference and future scenarios. The catchment-averaged soil loss projections are accompanied by percentages in parentheses. Values marked in bold are significantly different from zero ($p < 0.05$).

	Sierra de Segura			Guadalentín		
	reference (1981–2000)	near future (2031–2050)	far future (2081–2100)	reference (1981–2000)	near future (2031–2050)	far future (2081–2100)
RUSLE	418.2384	-15.1 (-3.6)	-153.6 (-36.7)	167.683	14.5 (8.7)	-21.4 (-12.8)
MUSLE	117.886	202.4 (171.7)	101.7 (86.3)	145.1148	213.7 (147.3)	122.9 (84.7)
MMF	88.169	38.2 (43.3)	11.1 (12.6)	121.3294	93.1 (76.7)	62.6 (51.6)

RUSLE: Revised Universal Soil Loss Equation; MUSLE: Modified Universal Soil Loss Equation; MMF: Morgan–Morgan–Finney.

In both catchments, the soil loss rates from RUSLE correlate with a combination of annual precipitation sum (Figure 3) and slope (Figure 1c), whereas the spatial pattern from MUSLE mostly coincides with the locations where most water accumulates. On the contrary, MMF shows a difference between the two catchments. In the Sierra de Segura catchment, most soil loss is projected in the eastern part of the catchment and shows similarity with the results from RUSLE for this part of the catchment. In the Guadalentín catchment, most soil loss is projected in the grid cells where most water accumulates, similar to the results from MUSLE. The spatial patterns obtained from the three models are inherently a result of the processes and environmental variables accounted for by the models, in which RUSLE is precipitation and slope dominated, MUSLE is dominated by accumulated runoff and MMF is a combination of the two.

The catchment-averaged annual soil loss for the reference scenario also differs between the three models (Table 6). The highest soil loss rates are projected by RUSLE, followed by MUSLE and MMF. In the case of the Sierra de Segura catchment, the catchment-averaged soil loss rate from RUSLE is almost five times that from MMF. RUSLE projects a higher catchment-averaged soil loss in the Sierra de

Segura catchment than in the Guadalentín catchment, whereas both MUSLE and MMF project an opposite response. Note that the soil loss rates as shown in Table 6 differ from the soil loss rates as shown in Table 4. The latter shows the unit soil loss corrected for plot length and slope gradient, which leads to lower soil loss rates in most cases.

Under climate change, the three models project considerable differences in spatial pattern and catchment-averaged soil loss. Although the spatial patterns show both significant increases and decreases in soil loss, RUSLE projects a decrease in catchment-averaged soil loss in the Sierra de Segura catchment for both scenarios and in the Guadalentín catchment for the far future scenario. A significant decrease in catchment-averaged soil loss is projected in the Sierra de Segura catchment for the far future scenario. MUSLE projects a significant increase in soil loss in both catchments and for both scenarios, with the greatest increase projected in locations where most water accumulates. MMF projects a significant increase in soil loss in the Sierra de Segura catchment for the near future scenario and a significant increase in the Guadalentín catchment for both scenarios. The results in the Guadalentín catchment show large similarities with results from MUSLE.

MMF includes three soil erosion processes: detachment by raindrop impact (equation (17)); detachment by runoff (equation (19)); and immediate deposition (equation (20)). The two detachment processes are directly affected by changes in precipitation (intensity) and runoff. In the reference scenario, most soil loss is produced from raindrop impact (Figure 5 and Table 7), with a raindrop impact–runoff ratio of up to 1.2 in the Sierra de Segura catchment. In both catchments and scenarios, detachment by raindrop impact is projected to significantly decrease and detachment by runoff is projected to significantly increase. Hence, in the projections with MMF, soil erosion shifts from raindrop impact dominated to runoff dominated, most notably for the near future scenario.

IV Discussion

The three soil erosion models evaluated here project a distinct impact of climate change on soil loss. Generally speaking, RUSLE projects a decrease in soil loss and MUSLE and MMF project an increase in soil loss (Table 6). The results from RUSLE and MUSLE show large similarities with, respectively, detachment from raindrop impact and detachment from runoff as projected by MMF (Figure 5). The decrease in soil loss as projected by RUSLE is largely the result of the projected decrease in annual precipitation sum, leading to a decrease in the rainfall erosivity (R factor). In some areas, an increase in soil loss is projected, most notably in the Guadalentín catchment. This is the result of a profound change in the intra-annual precipitation distribution towards a higher concentration of annual precipitation falling in only one or two months of the year. This affects the rainfall erosivity through the calculation of the MFI (equation (3)), which is a non-linear function that gives most importance to the months with high precipitation sums. Hence, under specific conditions, RUSLE is able to project increases in soil loss as a result of changes in the

(monthly) precipitation distribution. The detachment by raindrop impact from MMF also largely reflects the decrease in the annual precipitation sum, however, in some areas an increase is projected (Figure 5). This is mostly the result of changes in the precipitation intensity, which affects the calculation of the kinetic energy by direct throughfall (equation (18)). This is also a non-linear function and, hence, an increase in extreme precipitation may also result in an increase in the detachment by raindrop impact. This is particularly the case in the Guadalentín catchment, in which the areas where extreme precipitation increases (Figure 3) coincide with the areas where an increase in detachment by raindrop impact is projected, most notably in the south-eastern part of the catchment. In the Sierra de Segura catchment, a modest increase in extreme precipitation is projected, however, in this catchment detachment by raindrop impact is mostly affected by the decrease of annual precipitation sum.

In RUSLE, the rainfall erosivity is the only factor that will be affected by climate change. We estimated the rainfall erosivity based on the MFI , which is forced by the average monthly precipitation, following the equation by Renard and Freimund (1994). We apply this particular method here because it is the most applied method for estimating the R factor among the climate change impact studies (Table S1), even though these studies apply this empirical equation outside the USA where the data for this equation were obtained. Originally, the rainfall erosivity (EI_{30}) was defined as a multiplication of two factors: the rainfall energy (E) and the maximum continuous 30-minute intensity during an individual storm (I_{30}) (Wischmeier and Smith, 1958). Sub-hourly precipitation data are required to apply the original rainfall erosivity equation, which is often not available at large spatial scales. Therefore, statistical methods have been developed that relate observed monthly (e.g. Panagos et al., 2017) or daily (e.g. Beguería et al., 2018) precipitation to

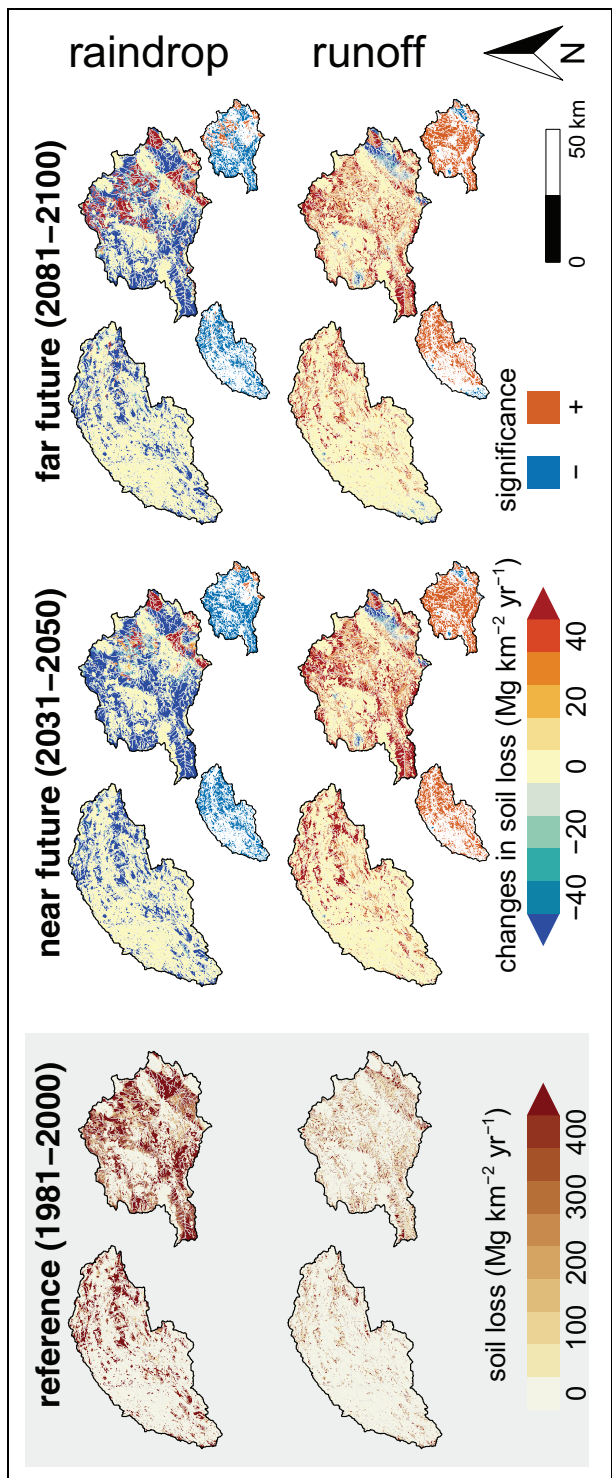


Figure 5. Ensemble average annual soil loss ($\text{Mg km}^{-2} \text{yr}^{-1}$) for the two soil erosion processes from MMF, that is, detachment by raindrop impact and detachment by runoff, for the reference scenario (1981–2000 left) and changes between the reference scenario and the two future scenarios (2031–2050 middle; 2081–2100 right). The small maps in the bottom right-hand corner of each map represent the significance, where blue indicates a significant decrease and red a significant increase ($p < 0.05$).

Table 7. Catchment-averaged annual soil loss ($\text{Mg km}^{-2} \text{yr}^{-1}$) for the two soil erosion processes from MMF, that is, detachment by raindrop impact and detachment by runoff, from the reference scenario and difference between the reference and future scenarios. The catchment-averaged soil loss projections are accompanied by percentages in parentheses. Values marked in bold are significantly different from zero ($p < 0.05$).

	Sierra de Segura			Guadalentín		
	reference (1981–2000)	near future (2031–2050)	far future (2081–2100)	reference (1981–2000)	near future (2031–2050)	far future (2081–2100)
raindrop	309.3	-169.5 (-54.8)	-157.1 (-50.8)	424.1	-164.2 (-38.7)	-88.8 (-21.0)
runoff	255.5	283.7 (111.0)	144.8 (56.7)	395.3	576.3 (145.8)	376.7 (95.3)
ratio	1.21	0.26	0.38	1.07	0.27	0.43

rainfall erosivity. Subsequently, these methods can be applied in climate change assessment studies, for which daily precipitation data are available from climate models. However, our literature review revealed that all the RUSLE-based studies used monthly or annual precipitation to determine rainfall erosivity under climate change (Table S1), most likely because of the lack of sub-hourly precipitation observations. As we have shown here, a shift in the monthly precipitation distribution may still lead to an increase in rainfall erosivity, even under a decreasing annual precipitation sum. However, the spatial pattern does not coincide with the spatial pattern of the change in extreme precipitation. For example, with RUSLE, an increase in soil loss is projected in the south-western part of the Guadalentín catchment for the near future scenario (Figure 4), where extreme precipitation is projected to decrease (Figure 3). Hence, monthly time steps may not be sufficient to infer the change in precipitation intensity that causes increased erosion under climate change (Nearing et al., 1990).

MUSLE projects a significant increase in soil loss in both catchments and scenarios, apart for some areas in the Guadalentín catchment. Similar results are obtained from detachment by runoff from MMF. Although the modest increase in extreme precipitation did not affect the detachment by raindrop impact in the Sierra

de Segura catchment, it does significantly affect the runoff as determined by the hydrological model and, hence, leads to an increase in projected soil loss by MUSLE and detachment by runoff by MMF. Extreme precipitation affects runoff generation because the SPHY hydrological model accounts for infiltration excess surface runoff, which depends largely on precipitation intensity. Admittedly, the hydrological model most likely underestimates high flow events (Figure 2), which may lead to an underestimation of soil loss for extreme events by MUSLE and MMF. Accounting for runoff-generated soil erosion should lead to improved soil loss projections, however, such models are largely dependent on the hydrological model used for simulation of (surface) runoff. Although the SPHY hydrological model accounts for many important processes, such as vegetation dynamics and infiltration excess surface runoff, it is still a huge challenge to apply and calibrate such models at large spatial scales (Blöschl et al., 2019; Sivapalan, 2018).

Oddly, the soil loss projections by MUSLE do not reflect differences between the two catchments, whereas for each of the two scenarios a similar catchment-averaged increase is projected (Table 6). On the contrary, MMF projects a dissimilar catchment-averaged increase in detachment by runoff between the two catchments, most notably in the far future scenario,

where the relative increase in the Guadalentín catchment is almost double that of the Sierra de Segura catchment. This is due to the characteristics of the two catchments, which are more explicitly reflected by MMF than by MUSLE. The Sierra de Segura catchment is characterized by natural vegetation and steeper slopes, which leads to higher ground cover values in MMF. The ground cover is a combination of the vegetation ground cover (Table 3) and rock cover, the latter increasing with slope steepness (Poesen et al., 1998). In the Sierra de Segura catchment, MMF often assumes a ground cover close to or equal to 1 in the case of steep slopes and natural vegetation, which leads to very low soil loss. Hence, a projected increase in runoff under climate change will not have such a significant effect on the detachment by runoff. In the Guadalentín catchment, this effect is not so strong because of generally lower slopes and less natural vegetation and, hence, lower ground cover. MUSLE is more sensitive for increases of runoff on steeper slopes because it does not explicitly account for ground cover by vegetation and rocks, but does this more implicitly through the *C* factor and the *CFRG* factor.

The results from the three models clearly show that climate change may have a distinct impact on soil erosion processes in the study area, with a projected decrease in soil loss as a result of decreasing annual precipitation sum and a projected increase in soil loss as a result of increasing runoff. Obviously, models that are either forced by precipitation or runoff, such as RUSLE and MUSLE, project a decrease or an increase in the study area. MMF is forced by both precipitation and runoff through the two considered soil erosion processes. The individual results of detachment by raindrop impact and runoff show considerable similarities with RUSLE and MUSLE, respectively. However, the resulting soil loss from MMF depends largely on the ratio between the two processes. It is unknown which of the two is the most dominant soil erosion process in the study area.

Through calibration of the detachability of the soil by raindrop impact (*K* in equation (17)) and runoff (*DR* in equation (19)) the ratio between the two soil erosion processes can be adjusted. The importance of a given process will affect the resulting soil loss under climate change.

V Conclusions

We assessed how soil erosion model conceptualization affects soil loss projections under climate change. In the study area, climate change is projected to cause a significant decrease in the annual precipitation sum, but also an increase in extreme precipitation. This contradicting climate signal has a profound impact on soil loss projections by the three models. On average, RUSLE projects decreasing soil loss, whereas MUSLE and MMF project soil loss to increase. The decrease in soil loss as projected by RUSLE is mainly the result of a decrease in the annual precipitation sum. In some areas, an increase is projected by this model, not necessarily, however, in areas where extreme precipitation is expected to increase. The results from RUSLE show large similarities with the results from the detachment by raindrop impact from MMF, which, similarly, is projected to decrease on average. Hence, we argue that soil erosion models that are forced by precipitation only, do not account sufficiently for the impact of changes in extreme precipitation on runoff, leading to an underestimation of soil loss under climate change.

On the contrary, MUSLE projects a significant increase in soil loss throughout the study area. These results show large similarities with results from the detachment by runoff from MMF, which also projects an increase. By accounting for both soil erosion processes, MMF projects a more balanced result, in which a projected decrease in detachment by raindrop impact, driven by the annual precipitation sum, is counteracted by a projected increase in detachment by runoff, which is driven by

extreme precipitation. Although it remains difficult to validate future soil erosion predictions, we argue that the impact of climate change on soil erosion can best be assessed with a soil erosion model that is forced by both precipitation and runoff. This is particularly the case for study areas where opposing changes in the annual precipitation sum and extreme precipitation are projected, which may have a contrasting effect on the two soil erosion processes.

Declaration of conflicting interests

The author(s) declared no potential conflicts of interest with respect to the research, authorship and/or publication of this article.

Funding

The author(s) disclosed receipt of the following financial support for the research, authorship, and/or publication of this article: J.P.C. Eekhout and J. de Vente acknowledge funding from the ‘Juan de la Cierva’ program (FJCI-2016-28905) and ‘Proyecto Intramural’ (201740I024) of the Spanish ‘Ministerio de Economía y Competitividad’.

ORCID iD

Joris P.C. Eekhout  <https://orcid.org/0000-0003-2097-696X>

Supplemental material

Supplemental material for this article is available online.

References

- Amanambu AC, et al. (2019) Spatio-temporal variation in rainfall-runoff erosivity due to climate change in the Lower Niger Basin, West Africa. *CATENA* 172: 324–334.
- Angulo-Martínez M, et al. (2016) Use of disdrometer data to evaluate the relationship of rainfall kinetic energy and intensity (KE-I). *Science of the Total Environment* 568: 83–94.
- Arnold JG, et al. (2012) SWAT: Model use, calibration, and validation. *Asabe* 55(4): 1491–1508.
- Arnoldus HMJ (1977) Methodology used to determine the maximum potential average annual soil loss due to sheet and rill erosion in Morocco. *FAO Soils Bulletin* 34: 39–48.
- Beasley LF, et al. (1980) ANSWERS: A model for watershed planning. *Transactions of the ASAE* 23(4): 0938–0944.
- Beguería S, et al. (2018) Computation of rainfall erosivity from daily precipitation amounts. *Science of the Total Environment* 637–638: 359–373.
- Bhuyan SJ, et al. (2002) Soil loss predictions with three erosion simulation models. *Environmental Modelling & Software* 17(2): 135–144.
- Blöschl G, et al. (2019) Twenty-three unsolved problems in hydrology (UPH): A community perspective. *Hydrological Sciences Journal* 64(10): 1141–1158.
- Borrelli P, et al. (2017) An assessment of the global impact of 21st century land use change on soil erosion. *Nature Communications* 8(1): 2013.
- Brown LC and Foster GR (1987) Storm erosivity using idealized intensity distributions. *Transactions of the ASAE* 30(2): 0379–0386.
- Bussi G, et al. (2014) Distributed sediment yield modeling: Importance of initial sediment conditions. *Environmental Modelling & Software* 58: 58–70.
- Centeri C, et al. (2009) Comparison of EUROSEM, WEPP, and MEDRUSH model calculations with measured runoff and soil-loss data from rainfall simulations in Hungary. *Journal of Plant Nutrition and Soil Science* 172(6): 789–797.
- Cerdan O, et al. (2002) Incorporating soil surface crusting processes in an expert-based runoff model: Sealing and transfer by runoff and erosion related to agricultural management. *CATENA* 46(2–3): 189–205.
- Chandramohan T, et al. (2015) Evaluation of three soil erosion models for small watersheds. *Aquatic Procedia* 4: 1227–1234.
- Chow VT (1959) *Open-channel Hydraulics*. New York: McGraw-Hill.
- Correa SW, et al. Soil erosion risk associated with climate change at Mantaro River basin, Peruvian Andes. *CATENA* 147: 110–124.
- Coulthard TJ and Van De Wiel MJ (2007) Quantifying fluvial non linearity and finding self organized criticality? Insights from simulations of river basin evolution. *Geomorphology* 91(3–4): 216–235.
- Croke J and Nethery M (2006) Modelling runoff and soil erosion in logged forests: Scope and application of some existing models. *CATENA* 67(1): 35–49.
- Desmet PJJ and Govers G (1996) A GIS procedure for automatically calculating the USLE LS factor on

- topographically complex landscape units. *Journal of Soil and Water Conservation* 51(5): 427–433.
- Eekhout JPC and Vente J (2019) The implications of bias correction methods and climate model ensembles on soil erosion projections under climate change. *Earth Surface Processes and Landforms* 44(5): 1137–1147.
- Eekhout JPC, et al. (2018a) Why increased extreme precipitation under climate change negatively affects water security. *Hydrology and Earth System Sciences* 22(11): 5935–5946.
- Eekhout JPC, et al. (2018b) Assessing the large-scale impacts of environmental change using a coupled hydrology and soil erosion model. *Earth Surface Dynamics* 6(3): 687–703.
- Ewen J, et al. (2000) SHETRAN: Distributed river basin flow and transport modeling system. *Journal of Hydrologic Engineering* 5(3): 250–258.
- Farr TG, et al. (2007) The shuttle radar topography mission. *Reviews of Geophysics* 45(2): RG2004.
- Gavrilović S (1972) Engineering on torrential streams and erosion. *Izgradnja* (Special Issue): 1–292.
- Gupta S and Kumar S (2017) Simulating climate change impact on soil erosion using RUSLE model: A case study in a watershed of mid-Himalayan landscape. *Journal of Earth System Science* 126(3): 43.
- Hengl T, et al. (2017) SoilGrids250 m: Global gridded soil information based on machine learning. *PLOS ONE* 12(2): e0169748.
- Herrera S, et al. (2016) Update of the Spain02 gridded observational dataset for EURO-CORDEX evaluation: Assessing the effect of the interpolation methodology. *International Journal of Climatology* 36(2): 900–908.
- Houska T, et al. (2015) SPOTting model parameters using a ready-made python package. *PLOS ONE* 10(12): 1–22.
- Jacob D, et al. (2014) EURO-CORDEX: New high-resolution climate change projections for European impact research. *Regional Environmental Change* 14(2): 563–578.
- Jetten V, et al. (2003) Erosion models: Quality of spatial predictions. *Hydrological Processes* 17(5): 887–900.
- Kerby W (1959) Time of concentration for overland flow. *Civil Engineering* 29(3): 174.
- Kirkby MJ (1988) Hillslope runoff processes and models. *Journal of Hydrology* 100(1–3): 315–339.
- Kirkby MJ, Abrahart R, McMahon M, et al. (1998) MEDALUS soil erosion models for global change. *Geomorphology* 24(1): 35–49.
- Kirkby MJ, Irvine BJ, Jones RJA, et al. (2008) The PESERA coarse scale erosion model for Europe. I – Model rationale and implementation. *European Journal of Soil Science* 59(6): 1293–1306.
- Kirpich ZP (1940) Time of concentration of small agricultural watersheds. *Civil Engineering* 10(6): 362.
- Ladson AR, et al. (2013) A standard approach to baseflow separation using the Lyne and Hollick Filter. *Australasian Journal of Water Resources* 17(1): 25–34.
- Lazar AN, et al. (2010) An assessment of the fine sediment dynamics in an upland river system: INCA-Sed modifications and implications for fisheries. *Science of the Total Environment* 408(12): 2555–2566.
- Liu Y, et al. (2019) Vulnerability assessment of the global water erosion tendency: Vegetation greening can partly offset increasing rainfall stress. *Land Degradation & Development* 30(9): 1061–1069.
- McCool DK, Brown LC, Foster GR, Mutchler CK and Meyer LD (1987) Revised Slope Steepness Factor for the Universal Soil Loss Equation. *Transactions of the ASAE* 30(5): 1387–1396.
- Maetens W, et al. (2012) Effects of land use on annual runoff and soil loss in Europe and the Mediterranean: A meta-analysis of plot data. *Progress in Physical Geography* 36(5): 599–653.
- Mahmoodabadi M and Sajjadi SA (2016) Effects of rain intensity, slope gradient and particle size distribution on the relative contributions of splash and wash loads to rain-induced erosion. *Geomorphology* 253(1): 159–167.
- Maina J, et al. (2013) Human deforestation outweighs future climate change impacts of sedimentation on coral reefs. *Nature Communications* 4(May): 1–7.
- MAPAMA (2010) Mapa de cultivos y aprovechamientos de España 2000–2010 (1: 50.000). Available at: www.magrama.gob.es/es/cartografia-y-sig/publicaciones/agricultura/mac_2000_2009.aspx (accessed 13 August 2019).
- Martínez-Murillo J, et al. (2013) Soil erosion and hydrology of the western Mediterranean badlands throughout rainfall simulation experiments: A review. *CATENA* 106: 101–112.
- Mondal A, et al. (2016) Impact assessment of climate change on future soil erosion and SOC loss. *Natural Hazards* 82(3): 1515–1539.
- Morgan RPC (2005) *Soil Erosion and Conservation*, 3rd ed. Malden, MA: Blackwell Science.

- Morgan RPC and Duzant JH (2008) Modified MMF (Morgan–Morgan–Finney) model for evaluating effects of crops and vegetation cover on soil erosion. *Earth Surface Processes and Landforms* 33(1): 90–106.
- Morgan RPC, et al. (1998) The European Soil Erosion Model (EUROSEM): A dynamic approach for predicting sediment transport from fields and small catchments. *Earth Surface Processes and Landforms* 23(6): 527–544.
- Nash JE and Sutcliffe JV (1970) River flow forecasting through conceptual models part I – A discussion of principles. *Journal of Hydrology* 10(3): 282–290.
- Nearing MA, Deer-Ascough L and Laflen JM (1990) Sensitivity analysis of the WEPP hillslope profile erosion model. *Transactions of the ASAE* 33(3): 0839–0849.
- Nearing MA, Foster GR, Lane LJ, et al. (1989) A process-based soil erosion model for USDA water erosion prediction project technology. *Transactions of the ASAE* 32(5): 1587–1593.
- Nearing MA, Pruski FF and O’Neal MR (2004) Expected climate change impacts on soil erosion rates: A review. *Journal of Soil and Water Conservation* 59(1): 43–50.
- Nearing MA, Wei H, Stone JJ, et al. (2011) A rangeland hydrology and erosion model. *Transactions of the ASABE* 54(3): 901–908.
- Nunes JP, et al. (2005) Evaluating the MEFIDIS model for runoff and soil erosion prediction during rainfall events. *CATENA* 61(2–3): 210–228.
- Panagos P, Ballabio C, Meusburger K, et al. (2017) Towards estimates of future rainfall erosivity in Europe based on REDES and WorldClim datasets. *Journal of Hydrology* 548: 251–262.
- Panagos P, Borrelli P, Poesen J, et al. (2015) The new assessment of soil loss by water erosion in Europe. *Environmental Science & Policy* 54: 438–447.
- Phomcha P, et al. (2011) Predicting sediment discharge in an agricultural watershed: A case study of the Lam Sonthi watershed. *Science Asia* 37(1): 43–50.
- Poesen JW, et al. (1998) Variation of rock fragment cover and size along semiarid hillslopes: A case study from southeast Spain. *Geomorphology* 23(2–4): 323–335.
- Renard KG and Freimund JR (1994) Using monthly precipitation data to estimate the R-factor in the revised USLE. *Journal of Hydrology* 157(1–4): 287–306.
- Renard KG, et al. (1997) *Predicting Soil Erosion by Water: A Guide to Conservation Planning with the Revised Universal Soil Loss Equation (RUSLE)*. Agricultural Handbook No. 703. United States Department of Agriculture, Agricultural Research Service. Available at: www.ars.usda.gov/SP2UserFiles/Place/64080530/RUSLE/AH_703.pdf (accessed 13 August 2019).
- Saxton KE and Rawls WJ (2006) Soil water characteristic estimates by texture and organic matter for hydrologic solutions. *Soil Science Society of America Journal* 70(5): 1569–1578.
- Serrano-Notivoli R, et al. (2017) SPREAD: A high-resolution daily gridded precipitation dataset for Spain – an extreme events frequency and intensity overview. *Earth System Science Data* 9(2): 721–738.
- Shen ZY, et al. (2009) A comparison of WEPP and SWAT for modeling soil erosion of the Zhangjiachong Watershed in the Three Gorges Reservoir Area. *Agricultural Water Management* 96(10): 1435–1442.
- Shrestha B, et al. (2013) Impact of climate change on sediment yield in the Mekong River basin: A case study of the Nam Ou basin, Lao PDR. *Hydrology and Earth System Sciences* 17(1): 1–20.
- Sivapalan M (2018) From engineering hydrology to earth system science: Milestones in the transformation of hydrologic science. *Hydrology and Earth System Sciences* 22(3): 1665–1693.
- Stolpe NB (2005) A comparison of the RUSLE, EPIC and WEPP erosion models as calibrated to climate and soil of south-central Chile. *Acta Agriculturae Scandinavica Section B: Soil and Plant Science* 55(1): 2–8.
- Sun Y, et al. (2007) How often will it rain? *Journal of Climate* 20(19): 4801–4818.
- Switanek BM, et al. (2017) Scaled distribution mapping: A bias correction method that preserves raw climate model projected changes. *Hydrology and Earth System Sciences* 21(6): 2649–2666.
- Teng H, et al. (2018) Current and future assessments of soil erosion by water on the Tibetan Plateau based on RUSLE and CMIP5 climate models. *Science of the Total Environment* 635: 673–686.
- Terink W, et al. (2015) SPHY v2.0: Spatial processes in hydrology. *Geoscientific Model Development* 8(7): 2009–2034.
- Tiwari AK, et al. (2000) Evaluation of WEPP and its comparison with USLE and RUSLE. *Transactions of the ASAE* 43(5): 1129–1135.
- Tollner EW, et al. (1976) Suspended sediment filtration capacity of simulated vegetation. *Transactions of the ASAE* 19(4): 0678–0682.

- Williams JR (1995) The EPIC model. In: Singh VP (ed.) *Computer Models of Watershed Hydrology*. Highlands Ranch, CO: Water Resources Publications, 909–1000.
- Wischmeier WH and Smith DD (1958) Rainfall energy and its relationship to soil loss. *Transactions, American Geophysical Union* 39(2): 285–291.
- Wischmeier W and Smith D (1978) *Predicting Rainfall Erosion Losses*. Agricultural Handbook No. 537. United States Department of Agriculture, Agricultural Research Service. Available at: <https://naldc.nal.usda.gov/download/CAT79706928/PDF> (accessed 13 August 2019).
- Wischmeier WH, et al. (1971) A soil erodibility nomograph for farmland and construction sites. *Journal of Soil and Water Conservation* 26(5): 189–193.
- Zare M, et al. (2016) Simulation of soil erosion under the influence of climate change scenarios. *Environmental Earth Sciences* 75(21): 1405.
- Ziadat FM and Taimeh AY (2013) Effect of rainfall intensity, slope, land use and antecedent soil moisture on soil erosion in an arid environment. *Land Degradation & Development* 24(6): 582–590.